Mass change of the Antarctic ice sheet inferred from ICESat and CryoSat-2

ZHANG Baojun[1], WANG Zemin[1*], AN Jiachun[1] & LIU Yanxia[2]

[1] Chinese Antarctic Center of Surveying and Mapping, Wuhan University, Wuhan 430079, China;
[2] Wuhan Geomatics Institute, Wuhan 430022, China

Abstract   This study examined the mass change of the Antarctic ice sheet (AIS) based on ICESat and CryoSat-2 observations. We estimated the AIS exhibited mass losses of -101 ± 15 Gt·a^{-1} during the ICESat period (Sept–Nov 2003 to Sept–Oct 2009) and -186 ± 55 Gt·a^{-1} during the CryoSat-2 period (Jan 2011 to Dec 2015). Mass losses occurred mainly in the sectors of the Amundsen and Bellingshausen seas. Benefitting from the 30-d subcycle of CryoSat-2, we obtained monthly estimates of mass evolution. Considerable annual variations were observed in the mass evolution sequences and the climatological monthly mass evolution. Seasonal mass evolutions in the sectors of the Bellingshausen and Amundsen seas were found most representative of the annual variation. The geographical distribution characteristics of interannual AIS mass evolution were revealed by the annual average mass evolution sequences. During Jan 2011 to Dec 2015, the ice sheets in the sectors of the Bellingshausen and Amundsen seas, and the Totten Glacier, experienced increasingly rapid areal mass loss. An area of mass gain with a moderate rate of increase was found between Dronning Maud Land and Enderby Land. Rapid mass accumulation has occurred in a limited area of the Kamb Ice Stream.

Keywords   Antarctic ice sheet, mass change, mass evolution, ICEsat, CryoSat-2

1   Introduction

For several thousand years, through basal melting, iceberg calving, and snowfall, the Antarctic ice sheet (AIS) has maintained dynamic mass balance (Yan et al., 2015; Kennicutt et al., 2013; Rémy and Parouty, 2009). However, within the context of present global warming, this mass budget has become imbalanced. This imbalance, which has been observed over the past two decades by a number of studies, e.g., Rignot et al. (2011), Pritchard et al. (2012), and Shepherd et al. (2012), is contributing to current and future sea level change. For an accurate prediction of future sea level change, it is necessary to quantify the current rate of change of the AIS mass balance.

Three independent methods can be used to determine AIS mass change. The first is the mass-budget method, where AIS mass change is calculated by differencing the input/output of mass to/from the ice sheet (Wen et al., 2010; Rignot et al., 2008; Rignot, 2002). The second method, known as the gravity-change approach, infers AIS mass change based on temporal variation of earth's gravitational field (Harig and Simons, 2015; Velicogna and Wahr, 2013; Chen et al., 2009). The third approach is the volumetric method, in which AIS mass change is detected based on the variation of surface elevation as observed by satellite altimetry (radar and laser) (Zhang et al., 2017; Li et al., 2016; Zwally et al., 2015; Groh et al., 2014; Gunter et al., 2014; McMillan et al., 2014a; Zwally et al., 2012; Pritchard et al., 2009; Zwally et al., 2005). Most recent studies have indicated that the AIS is melting

---

* Corresponding author, E-mail: zmwang@whu.edu.cn

at a high rate and that this rate of melting is accelerating. For instance, Harig and Simons (2015) reported that the trend of total mass change of the AIS during 2003–2014 was −92±10 Gt·a^{-1}, with a rate of acceleration of −6±6 Gt·a^{-2}. The magnitude of this trend is within the bounds of error of other recent studies (Luthcke et al., 2013; Sasgen et al., 2013; Velicogna and Wahr, 2013). Over the last decade, West Antarctica, i.e., along the Amundsen Sea sector and the tip of the Antarctic Peninsula, has experienced a considerable rate of ice mass loss. Although snowfall in Dronning Maud Land has added ice mass to the continent, the accelerated rate of ice mass loss in West Antarctica continues to outpace gains made in East Antarctic regions. However, Zwally et al. (2015) reached a contrasting conclusion; they found that ice mass gain during 2003–2008 exceeded mass loss by 82±25 Gt·a^{-1}, which would have reduced global sea level rise by 0.23 mm·a^{-1}.

The Ice, Cloud, and Land Elevation Satellite (ICESat), launched in Jan 2003, was the first satellite laser altimeter mission. Between 2003 and 2009, its geoscience laser altimeter system acquired valuable altimetry data with unprecedented levels of accuracy and resolution (Zwally et al., 2012). The CryoSat-2 mission was launched in April 2010. Its main payload is the Synthetic Aperture Interferometric Radar Altimeter, which provides continuous observations up to latitudes of 88.0°N/°S. The novel synthetic aperture radar interferometry mode of CryoSat-2 is designed to improve the accuracy, resolution, and geolocation of its height measurements in areas of steep terrain and on the narrow margins of ice sheets (Wingham et al., 2006).

The independent datasets acquired by ICESat and CryoSat-2 constitute a valuable source of data for the study of the detailed pattern of AIS mass change since 2003. Benefitting from these observations, we quantified AIS mass change during 2003–2015 with high spatial resolution. The characteristics of AIS mass change were analyzed by comparison of the results from the two satellite altimeters. Previous studies have generally focused only on the rate of ice mass ablation, especially those based on ICESat measurements, which was observed two to three times annually following the compromised observation plan (discussed in Section 2). In fact, the mass change time series can also provide other important and meaningful information that could promote our understanding of the AIS mass balance. The spatiotemporal characteristics of the seasonal and interannual evolutions represent important research objects that could reveal the variations of the AIS. Benefitting from the 30-d subcycle observations of CryoSat-2, we calculated monthly estimates of AIS mass evolution, and the detailed pattern of AIS mass change between 2011 and 2015 was resolved using this monthly mass evolution series.

2　Data and methods

The latest releases of the ICESat dataset (GLA12, release 34) and the CryoSat-2 Level 2 product were used in this study. The ICESat dataset, which covers the period Sep–Nov 2003 to Sep–Oct 2009 with a 91-d repeated orbit, was provided by the National Snow and Ice Data Center. The preprocessing criteria adopted to cull and correct the ICESat measurements followed the methodology of Ewert et al. (2012a). The CryoSat-2 dataset, which covers the period from Jan 2011 to Dec 2015, was provided by the European Space Agency. We removed erroneous CryoSat-2 height records for which the quality flags indicated bad data or where the interferometric across-track location failed in the SARIn mode. After preprocessing, we adapted the methods as described below to compute AIS surface elevation change.

For ICESat observations, we fitted the surface height measurements in an area of 700 × 500 m^2 along the repeat tracks using a mathematical model from Ewert et al. (2012b), which is also similar to Pritchard et al. (2009), Moholdt et al. (2010), and Sorensen et al. (2011):

$$H_i = \bar{H} + \dot{H} \cdot t_i + f(x_i, y_i) + \varphi(t_i), \quad i = 1 \cdots N , \quad (1)$$

where i is the counter, N denotes the number of observations within each fitted bin, H_i denotes the surface elevation observation, $\bar{H}$ denotes the mean elevation in the bin center, $\dot{H}$ denotes the long-term surface elevation change, t_i denotes the time, and $f(x_i, y_i)$ denotes the surface fitting of the topography:

$$\begin{aligned} f(x_i, y_i) = &a_1 x_i + a_2 y_i + a_3 x_i y_i + a_4 x_i^2 \\ &+ a_5 y_i^2 + a_4 x_i^2 y_i + a_5 x_i y_i^2 + a_8 x_i y_i^2 \end{aligned}, \quad (2)$$

where x_i and y_i denote the projection coordinates in each bin, a_{1-8} are the coefficients of a biquadratic surface model accounting for topography, and $\varphi(t_i)$ denotes the seasonal signal given by:

$$\varphi(t_i) = A \cos\left(\frac{2\pi}{T} t_i\right) + B \sin\left(\frac{2\pi}{T} t_i\right), \quad (3)$$

with amplitude $S = \sqrt{A^2 + B^2}$ and period $T = 365$ d.

Deriving elevation changes from CryoSat-2 required a slightly different approach compared with that used for ICESat. This is because the repeat cycle (369 d) of CryoSat-2 is so long that the conventional repeat-track method is unsuitable. We grouped the CryoSat-2 records into 5 × 5 km^2 bins and estimated the linear rates of elevation change according to McMillan et al. (2014a). Because of the impact of snowpack anisotropy on surface heights derived by the radar altimeter, a time-invariant elevation offset exists between the ascending and descending orbits (Armitage et al., 2014). The impact of changing snowpack liquid water content, density, and roughness on the backscattered echo also has the potential to introduce artificial signals into the radar altimeter

elevation measurements (Flament and Rémy, 2012). To minimize the impacts of both the ascending–descending offset and the temporal changes of backscatter, we included additional terms in Eq. (1):

$$H_i = \bar{H} + \dot{H} \cdot t_i + f(x_i, y_i) + \varphi(t_i) + m\Lambda + nbs, \ i = 1 \cdots N, \quad (4)$$

where Λ relates to the satellite heading (assigned a value of 0 or 1 depending upon whether it was acquired on an ascending or a descending pass), m denotes the ascending–descending offset, bs denotes backscatter, and N is the number of observations within each fitted bin.
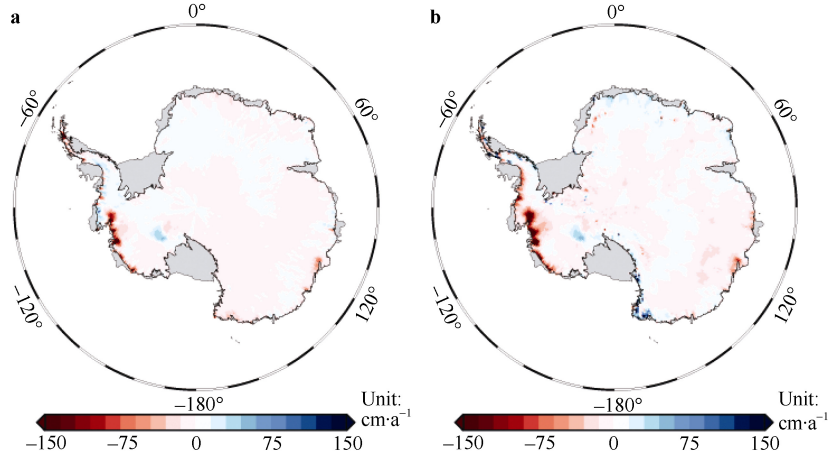

Figure 1   Surface elevation change rates without GIA correction: Sep–Nov 2003 to Sep–Oct 2009, as derived from ICESat (**a**) and Jan 2011 to Dec 2015, as derived from CryoSat-2 (**b**).
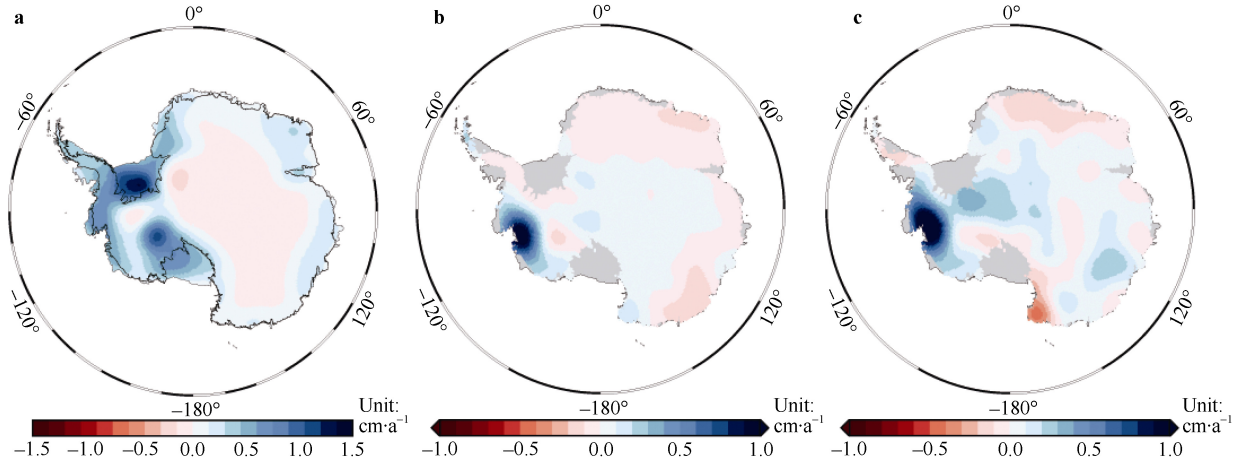

Figure 2   Model predictions of GIA-induced vertical crustal deformation according to ICE-6G_C (**a**). Elastic crustal deformations due to the ice mass change: Sep–Nov 2003 to Sep–Oct 2009 (**b**), as derived from ICESat and Jan 2011 to Dec 2015 (**c**), as derived from CryoSat-2.

Following the preprocessing, we used an iterative least squares estimator to retrieve the coefficients in Eq. (1) or Eq. (4) in each bin. We removed anomalous measurements for which the residuals were at least three times larger than the standard deviation. Parameters were then estimated using the remaining height measurements in each bin. The iteration continued until parameters were estimated from all the observations that passed the 3-σ test or until the remaining observations in the bin did not meet the thresholds. The thresholds for the ICESat data were that the number of observations in each bin had to be >18 and that they had to be from more than 6 passes (Liu et al., 2014;

Ewert et al., 2012b). The thresholds for the CryoSat-2 data were that the number of observations in each bin had to be >100 and that they had to have a time span of at least 2 years (McMillan et al., 2014a, 2014b).

The unexpectedly rapid energy decline and subsequent failure of Laser 1 of the ICESat mission produced nonnegligible systematic campaign bias. The bias was estimated in this study using surface height measurements obtained in the most arid region of East Antarctica, along the same lines as described by Gunter et al. (2014). The surface change of the firn in the region due to accumulation or compaction was estimated using the

Institute for Marine and Atmospheric Research Utrecht Firn Densification Model (IMAU-FDM) (Ligtenberg et al., 2011). This value was removed from the surface height change derived from ICESat observations in the region to derive the final campaign bias estimates. We estimated the campaign bias as 1.34 ± 0.06 cm·a^{-1}, which was subtracted from all surface elevation change rates. Figure 1 shows the elevation change rates of the AIS for the period Sep–Nov 2003 to Sep–Oct 2009, as derived from ICESat, and for the period from Jan 2011 to Dec 2015, as derived from CryoSat-2.

Although we adopted a robust least squares method to estimate the surface elevation change, some outliers remained. To minimize the impact of these outliers, we smoothed the estimated rates derived from both ICESat and

CryoSat-2 using a 30×30 km^2 median filter (Ewert et al., 2012b). The viscoelastic deformation of the solid earth due to glacial isostatic adjustment (GIA) and the elastic crustal deformation caused by present-day mass changes are also detected by ICESat. These are unrelated to ice volume change and thus, it was necessary to correct for these deformations to determine AIS mass changes. In this study, the elevation change rates were corrected for surface height changes due to GIA, as predicted by ICE-6G_C (Argus et al., 2014), shown in Figure 2a. The elastic crustal deformation can be calculated from the ice mass change based on Eq. (6), described by Groh et al. (2012). The elastic crustal deformation is shown in Figure 2b and Figure 2c, and it was removed from the estimated surface elevation change.
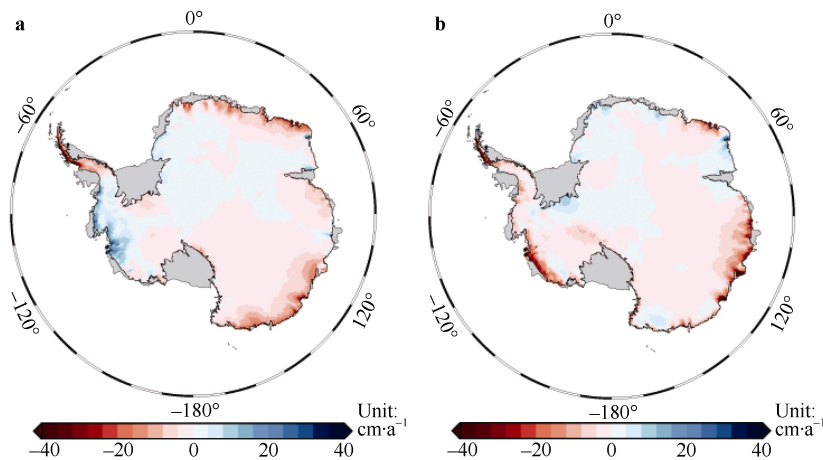

Figure 3 Rates of IMAU-FDM surface elevation changes: Sep–Nov 2003 to Sep–Oct 2009 (**a**) and Jan 2011 to Dec 2015 (**b**).
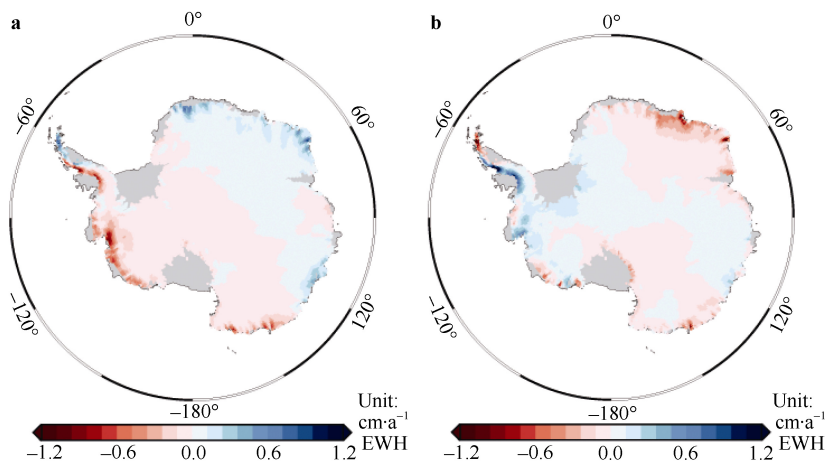

Figure 4 SMB mass change rates (in cm·a^{-1} equivalent water height (EWH)) simulated by RACMO2.3: Sep–Nov 2003 to Sep–Oct 2009 (**a**) and Jan 2011 to Dec 2015 (**b**).

We used the IMAU-FDM and Surface Mass Balance (SMB) simulated by RACMO2.3 (Lenaerts et al., 2012) to convert surface elevation changes to mass changes. The IMAU-FDM surface elevation changes are shown in Figure 3, and the SMB mass change rates are shown in Figure 4.

First, we subtracted the IMAU-FDM surface elevation changes from the observed ICESat and CryoSat-2 surface elevation changes to obtain the elevation change attributable to ice dynamical imbalance. Then, using the density of ice (i.e., 917 kg·m^{-3}), the residual elevation

change was translated to mass. Finally, we added back the SMB mass change over the same period to estimate the total mass change. The calculation used for the mass changes can be summarized as follows:

$$\dot{m}_{\text{ice}} = (\dot{H} - \dot{H}_{\text{FDM}} - \dot{H}_{\text{GIA}} - \dot{H}_{\text{ECD}}) \cdot \rho + \dot{m}_{\text{SMB}}, \qquad (5)$$

where $\dot{m}_{\text{ice}}$ denotes the mass change rate, $\dot{H}_{\text{FDM}}$ denotes the IMAU-FDM surface elevation change rate, $\dot{H}_{\text{GIA}}$ denotes the GIA-induced vertical crustal deformation rate, $\dot{H}_{\text{ECD}}$ denotes the elastic crustal deformation rate, ρ is the density of ice (917 kg·m^{-3}), and $\dot{m}_{\text{SMB}}$ denotes the SMB mass change rate. The uncertainties associated with the mass change estimates can be computed using formal error propagation techniques (McMillan et al., 2016; Gunter et al., 2014). The uncertainty of the mass rate (σ_{ice}) was estimated from the uncertainties of the individual input datasets as follows:

$$\sigma_{\text{ice}} = \sqrt{(\sigma_{\dot{H}}^2 + \sigma_{\text{FDM}}^2 + \sigma_{\text{GIA}}^2 + \sigma_{\text{ECD}}^2) \cdot \rho^2 + \sigma_{\text{SMB}}^2}, \qquad (6)$$

where $\sigma_{\dot{H}}$, σ_{FDM}, σ_{GIA}, σ_{ECD}, and σ_{SMB}^2 denote the uncertainties of $\dot{H}$, $\dot{H}_{\text{FDM}}$, $\dot{H}_{\text{GIA}}$, $\dot{H}_{\text{ECD}}$, and $\dot{m}_{\text{SMB}}$, respectively. Where possible, the uncertainties of the altimetry surface height changes were the associated interquartile ranges, while certain assumptions were made for other independent datasets, as described by Gunter et al. (2014) and by Riva et al. (2009), the details of which are outlined below. For IMAU-FDM surface elevation changes and SMB mass change rates, 10% of the value for each grid point was adopted as the uncertainty, referring to Gunter et al. (2014). For GIA corrections, 30% of the value for each grid point was used as the uncertainty, referring to Gao et al. (2015). The elastic crustal deformation was so small that we set 30% of its value for each grid point as its uncertainty to simplify the calculation.

Benefiting from the 30-d subcycle of CryoSat-2, we calculated the monthly estimates of AIS mass change. According to Eq. (4), the elevation anomalies ΔH_i can be obtained from CryoSat-2 for each bin by

$$\Delta H_i = H_i - (\bar{H} + \text{f}(x_i, y_i) + m\Lambda + nbs), i = 1 \cdots N. \qquad (7)$$

Then, by averaging the elevation anomalies within each month, the long-term time series for each bin can be obtained. However, the observations for each 30-d subcycle did not cover every bin, especially after outlier editing. Therefore, to obtain a continuous time series, we used interpolation to fill the empty bins. Before interpolation, to minimize the impact of gross errors, the monthly elevation anomalies were smoothed using a 30 × 30 km^2 median filter. Statistics indicate that <10% of the 30 × 30 km^2 cells needs to be filled by means of interpolation. With reference to Bamber et al. (2009), we considered that the 30-km spatial resolution, established by the interpolation method, could represent the true monthly mean elevation anomaly of the AIS. In this study, interpolation was performed using the tension spline surface interpolation method, developed by

Smith and Wessel (1990). By setting the tension parameter to 0.35, as described by Wessel et al. (2017), the value of the interpolation point preserves local characteristics and short wavelength information.

3 Results and discussion

3.1 Mass changes of the AIS

The ICESat-derived pattern of AIS mass change, shown in Figure 5a, reveals a mass change pattern consistent with that of many previous studies (Zhang et al., 2017; Zwally et al., 2015; Shepherd et al., 2012; Shi et al., 2011; Gunter et al., 2009). Between Sep–Nov 2003 and Sep–Oct 2009, the largest signal of mass loss occurred in the Amundsen Sea sector (basins 20, 21, and 22), which comprises the Pine Island Glacier, Thwaites and Smith glaciers, and glaciers flowing into the Getz Ice Shelf. Negative mass change signals also occurred on the Antarctic Peninsula (basins 25 and 26), Totten Glacier (basin 13), Demman Glacier (basin 12), and Cape Poinsett (basin 15). The largest positive signal of mass change was observed on the Kamb Ice Stream (basin 18). Slight mass gain was also observed in some coastal regions, e.g., Palmer Land (basin 24), Dronning Maud Land (basin 5), Enderby Land (basin 7), George V Land (basin 14), and Terre Adelie (basin 13). No significant mass change was observed in the Central East Antarctic over this period.

Figure 5b shows the AIS mass change trends over the CryoSat-2 period. The results derived from CryoSat-2 confirm continuation of the pattern observed by ICESat in many regions. During the CryoSat-2 period, the largest negative mass change signal was still observed in the Amundsen Sea sector (basins 20, 21, and 22), but it showed a higher rate than observed during the ICESat period. The Totten Glacier also exhibited a greater rate of mass loss than observed by ICESat. There are some areas where the mass change signals were reversed, e.g., the Bellingshausen Sea sector (basins 23 and 24). The widespread signals of mass loss across this area, derived from CryoSat-2, were significantly different from the observations acquired by ICESat, which mainly showed modest mass gains. Across the Central East Antarctic during the CryoSat-2 period, the mass change signals were slightly larger than during the ICESat period. It should be noted that this phenomenon might also be due to sensitivity to changes not corrected completely in the calculation. The signals of mass change in the Queen Maud Mountains and Victoria Land, along the Ross Sea and on the Ross Ice Shelf, and on Palmer Land along the Weddell Sea, might have been contaminated by errors caused by the steep terrain. It is considered that the derived significant signals of mass gain are not credible.

Differencing the CryoSat-2 mass change trends and the ICESat mass change trends allowed us to investigate the discrepancies between the two mass change budgets (Figure 5c). The largest increases of mass loss occurred for glaciers flowing into the ice shelf along the Bellingshausen Sea
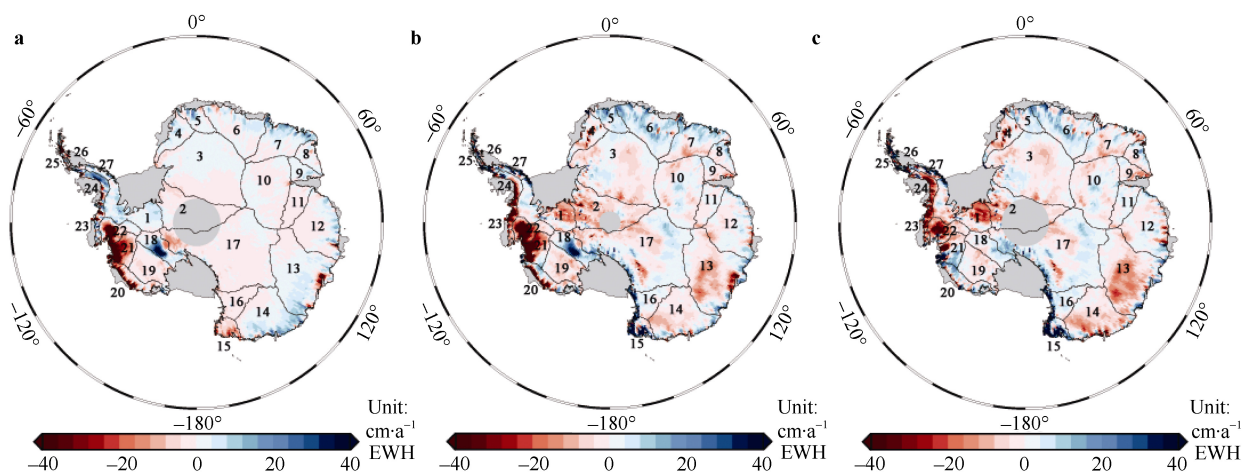
Figure 5   Rate of AIS mass change: Sep–Nov 2003 to Sep–Oct 2009 (ICESat) (**a**) and Jan 2011 to Dec 2015 (CryoSat-2) (**b**). Difference between the derived mass changes of the two periods. Solid black lines show the boundaries of the 27 ice sheet drainage basins (Zwally et al., 2012) (**c**).

coast (basins 23 and 24), on the Pine Island Glacier (basin 22), and on the Thwaites and Smith glaciers (basin 21). These accelerations might be attributable to accelerated ice discharge of the ice sheet (Gardner et al., 2017). Modest acceleration of mass loss was found in George V Land (basin 14), Terre Adelie (basin 13), and the region between Edith Ronne Land and the Ellsworth Mountains (basin 1). The greatest acceleration of mass loss was found in the region between Dronning Maud Land and Enderby Land (basin 6), ignoring those areas potentially contaminated by errors related to steep terrain.

Table 1 shows the mass change rates of all the drainage basins for both the ICESat and the CryoSat-2 periods. When integrated across the entire AIS, the total mass loss rate for the ICESat period was -101 ± 15 Gt·a^{-1}. In the West Antarctica Ice Sheet (WAIS; basins 1 and 18–23), East Antarctica Ice Sheet (EAIS; basins 2–17), and Antarctic Peninsula Ice Sheet (APIS; basins 24–27), the rates of mass change during the ICESat period were -90 ± 10, 31 ± 6, and -11 ± 8 Gt·a^{-1}, respectively. The total mass loss rate over the CryoSat-2 period was $-186\pm$

55 Gt·a^{-1}. In the WAIS, EAIS, and APIS, the rates of mass change were -197 ± 20, -9 ± 45, and 12 ± 25 Gt·a^{-1}, respectively. These estimates of mass change agree with the recent study by Groh et al. (2014) (-126 ± 20 Gt·a^{-1} for the ICESat period) and the recent study by McMillan et al. (2016) (-159 ± 48 Gt·a^{-1} for the CryoSat-2 period) using a similar study period and the same observations. The Cryosat-2 observations revealed a greater rate of mass loss for the AIS than derived from ICESat, particularly in areas of the Amundsen Sea sector (-149 ± 10 Gt·a^{-1} for the ICESat period; 168 ± 12 Gt·a^{-1} for the CryoSat-2 period) and the Bellingshausen Sea sector (-3 ± 4 Gt·a^{-1} for the ICESat period; 20 ± 3 Gt·a^{-1} for the CryoSat-2 period). It should be noted that some studies have used ICESat data to draw conclusions that contrast with this work, e.g., Zwally et al. (2015). Zwally et al. (2015) reached the conclusion that "mass gains of the Antarctic ice sheet exceed losses". Based on consideration of the discussion of Zwally et al. (2015), we suggest that the use of different SMB and FDM models is an important reason for the inconsistent conclusions.

Table 1   Basin ID, mean elevation rate, and mass change rate of Antarctic drainage basins for Sep–Nov 2003 to Sep–Oct 2009 (ICESat period) and Jan 2011 to Dec 2015 (CryoSat-2 period)

Basin	Area[a] /(10^6·km^2)	ICESat		CryoSat-2	
		Mean elevation rate/(cm·a^{-1})	Mass change rate /(Gt·a^{-1})	Mean elevation rate /(cm·a^{-1})	Mass change rate /(Gt·a^{-1})
2	0.66[b]	-0.7 ± 0.1	-5 ± 1	-5.4 ± 0.3	-38 ± 13
3	1.57	0.8 ± 0.1	-1 ± 1	-1.1 ± 0.2	-18 ± 12
4	0.24	4.3 ± 0.2	4 ± 1	-1.9 ± 1.8	-5 ± 16
5	0.19	0.4 ± 0.2	5 ± 1	8.9 ± 1.2	12 ± 5
6	0.61	-2.5 ± 0.2	7 ± 1	6.0 ± 1.3	32 ± 11
7	0.49	-1.5 ± 0.4	17 ± 3	-0.7 ± 1.0	10 ± 7
8	0.16	0.2 ± 0.3	1 ± 1	4.7 ± 2.2	0 ± 5

(Continued)

Basin	Area[a] /(10⁶·km²)	ICESat		CryoSat-2	
		Mean elevation rate/(cm·a⁻¹)	Mass change rate /(Gt·a⁻¹)	Mean elevation rate /(cm·a⁻¹)	Mass change rate /(Gt·a⁻¹)
9	0.14	3.9±0.2	3±1	0.5±1.5	−3±5
10	0.92	0.2±0.1	−2±1	−1.5±0.3	−4±5
11	0.26	−2.6±0.1	−3±1	−0.4±0.8	−1±6
12	0.72	−1.8±0.2	2±2	−5.3±0.6	0±7
13	1.11	−3.0±0.1	15±2	−8.8±0.7	−41±7
14	0.72	−2.4±0.2	23±2	−3.1±0.7	−13±5
15	0.12	−14.2±1.1	−12±2	31.0±9.6	37±24
16	0.27	−2.7±0.2	−5±1	6.4±1.9	20±14
17	1.84[c]	−2.0±0.1	−17±2	−0.5±0.5	4±17
EAIS	10.03	−1.3±1.3	31±6	−1.3±10.6	−9±45
1	0.49	3.8±0.3	19±2	−0.9±1.4	−14±16
18	0.27	6.7±0.2	19±1	7.5±0.4	26±2
19	0.37	−2.0±0.2	−6±1	−4.5±0.6	−14±3
20	0.19	−12.6±0.4	−25±5	−22.2±2.1	−17±6
21	0.22	−29.2±0.3	−79±7	−42.5±1.0	−76±8
22	0.22	−17.1±0.3	−45±4	−38.4±0.9	−75±5
23	0.08	7.5±0.7	−3±4	−32.1±2.0	−20±3
WAIS	1.83	−4.9±1.0	−90±10	−13.3±3.6	−197±20
24	0.10	6.4±1.7	6±5	−16.9±3.0	−11±8
25	0.04	−52.4±5.2	−8±5	16.8±18.5	12±15
26	0.04	−39.5±3.8	−12±4	4.5±12.7	3±15
27	0.05	−1.3±1.3	3±2	12.5±6.0	8±11
APIS	0.23	−12.88±6.8	−11±8	−0.90±23.5	12±25
AIS	12.08	−2.08±7.0	−101±15	−3.07±26.0	−186±55

Notes: [a]Areas of basins listed are spatial coverages observed by CryoSat-2; [b]Area of basin 2 observed by ICESat is 0.35 × 10⁶ km²; [c]Area of basin 17 observed by ICESat is 1.66 × 10⁶ km².

3.2 Mass evolution of the AIS from CryoSat-2

Benefiting from the 30-d subcycle of the CryoSat-2 mission, we produced a monthly time series of mass change. Figure 6a shows the monthly mass evolution and its linear trend between Jan 2011 and Dec 2015, together with the corresponding series of SMB and CryoSat-2–SMB difference. Figure 6b shows the energy spectra corresponding to the three times series of mass evolution. The CryoSat-2 series represents the monthly mass change derived from CryoSat-2 measurements, i.e., the total monthly mass change caused by the sum of the surface balance and the dynamic mass change. The SMB series represents the monthly average surface balance simulated by RACMO2.3. The CryoSat-2–SMB series is defined as the difference between the total monthly mass change (CryoSat-2) and the monthly average surface balance

(SMB), when the SMB mass changes simulated by RACMO2.3 were reliable (McMillan et al., 2016). The mean values of the three times series of mass evolution have been removed. The pattern shown in Figure 5b reveals rapid mass loss across the AIS during the CryoSat-2 period in Figure 6a, while the SMB shows almost no change. The mass loss of the AIS could be attributed almost entirely to dynamic processes. From Figure 6b, significant annual variation can be seen in each mass evolution sequence. The annual amplitude of the SMB mass change is smaller than that of the mass change derived from CryoSat-2. Because the annual phase of the SMB is the inverse of the mass change derived from CryoSat-2, the annual amplitude of mass change due to dynamic processes (i.e., CryoSat-2–SMB) is greater than that of the SMB mass change or the mass change derived from CryoSat-2.

We calculated the climatological monthly mass

evolution over the same month from Jan 2011 to Dec 2015, obtaining one map for each month, which revealed evident spatial climatological monthly variations in mass distribution (Figure 7). The ice sheet began losing mass in September in the sectors of the Bellingshausen and Amundsen seas, where the largest signals of mass loss were found. Over time, the mass loss signal reached a maximum in January. Then, after a period of rapid mass accumulation, the rate of accumulation diminished gradually until it disappeared in June. The mass change in

these regions is caused mainly by dynamic processes (Hogg et al., 2017; Zwally et al., 2015; Mouginot et al., 2014; Sutterley et al., 2014). Therefore, we speculate that the annual mass change in these regions was related primarily to the annual variation of sea ice or the ice shelf. Certainly, this conjecture needs to be explored in future studies. The SMB mass change also plays a very important role in the seasonal variation of AIS mass change, especially on the coast of the EAIS (Harig and Simons, 2015; Ki-Weon et al., 2015; Boening et al., 2012).
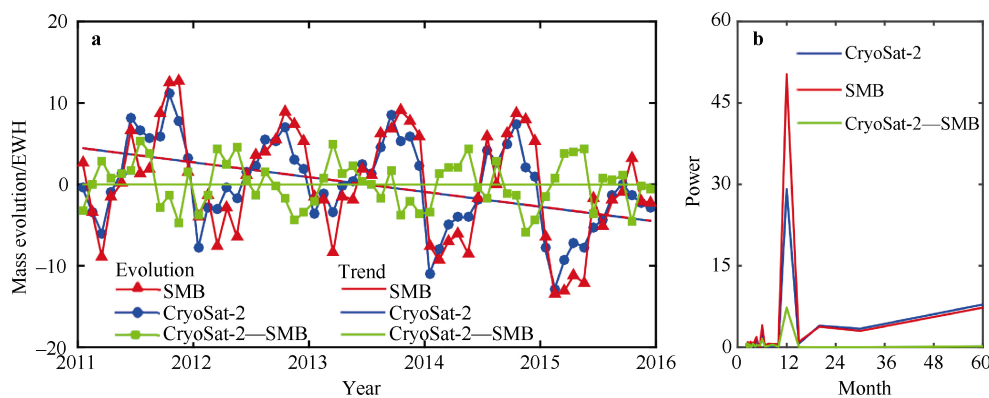

Figure 6　Monthly mass evolution of the AIS between Jan 2011 and Dec 2015, as derived from CryoSat-2, with corresponding SMB and CryoSat-2–SMB difference (**a**), and the corresponding energy spectra (**b**).

The annual average mass evolution was calculated on an annual basis by averaging data from 2011 to 2015. The annual mean maps of mass anomaly, relative to the average during the period from Jan 2011 to Dec 2015, are shown in Figure 8. The area of mass loss increased in the sectors of the Bellingshausen and Amundsen seas during 2011–2015. An analogous situation also occurred at the Totten Glacier. Moderate mass gain occurred in the area between Dronning Maud Land and Enderby Land. The Kamb Ice Stream showed the largest mass gain over the five-year period, although the mass gain was limited to a specific area. At the same time, northern parts of the Antarctic Peninsula experienced repeated periods of mass loss and gain.

4　Conclusions

Using ICESat (laser) and CryoSat-2 (radar) altimetry observations in conjunction with the RACMO2.3 and IMAU-FDM models, we computed the AIS mass change over the periods of Sep–Nov 2003 to Sep–Oct 2009 and Jan 2011 to Dec 2015. Our results showed that the AIS experienced an average mass loss of -101 ± 15 Gt·a^{-1} (WAIS: -121 ± 10 Gt·a^{-1}, EAIS: 31 ± 6 Gt·a^{-1}, APIS: -11 ± 8 Gt·a^{-1}) over the ICESat period. During this time, mass loss occurred in the Amundsen Sea sector, at the tip of the Antarctic Peninsula, and on the Totten and Demman glaciers and on Cape Poinsett. Mass was gained in the Kamb Ice Stream and some coastal regions of the AIS.

CryoSat-2 confirmed continuation of the negative mass balance estimated by the ICESat mission for many regions, e.g., the largest rate of mass loss occurred in the Amundsen Sea sector and the greatest rate of mass gain was in the Kamb Ice Stream. Some differences were found between the two periods. For example, the mass change signal in the Bellingshausen Sea sector was reversed between the two periods, and accelerations of mass change occurred in many regions, such as the Pine Island Glacier, Thwaites and Smith glaciers, and areas between Dronning Maud Land and Enderby Land. Compared with the observations acquired by ICESat, the Cryosat-2 observations revealed an accelerated rate of mass loss for the AIS, which was attributable primarily to the accelerated rate of mass loss in the sectors of the Amundsen and Bellingshausen seas. The rate of AIS ice mass change was -186 ± 55 Gt·a^{-1} (WAIS: -190 ± 20 Gt·a^{-1}, EAIS: -9 ± 45 Gt·a^{-1}, APIS: 12 ± 25 Gt·a^{-1}) over the CryoSat-2 period.

We estimated the monthly mass evolution of the AIS between Jan 2011 and Dec 2015. Significant annual variation was found in the monthly mass sequences and in the climatological mass evolution. For example, in the sectors of the Bellingshausen and Amundsen seas, mass loss began in September and reached its maximum in January. Then, after a period of rapid mass accumulation, the rate of accumulation diminished gradually until it disappeared in June. The annual average mass evolution during the period revealed that the ice sheet in the sectors of the Bellingshausen and Amundsen seas and the Totten Glacier
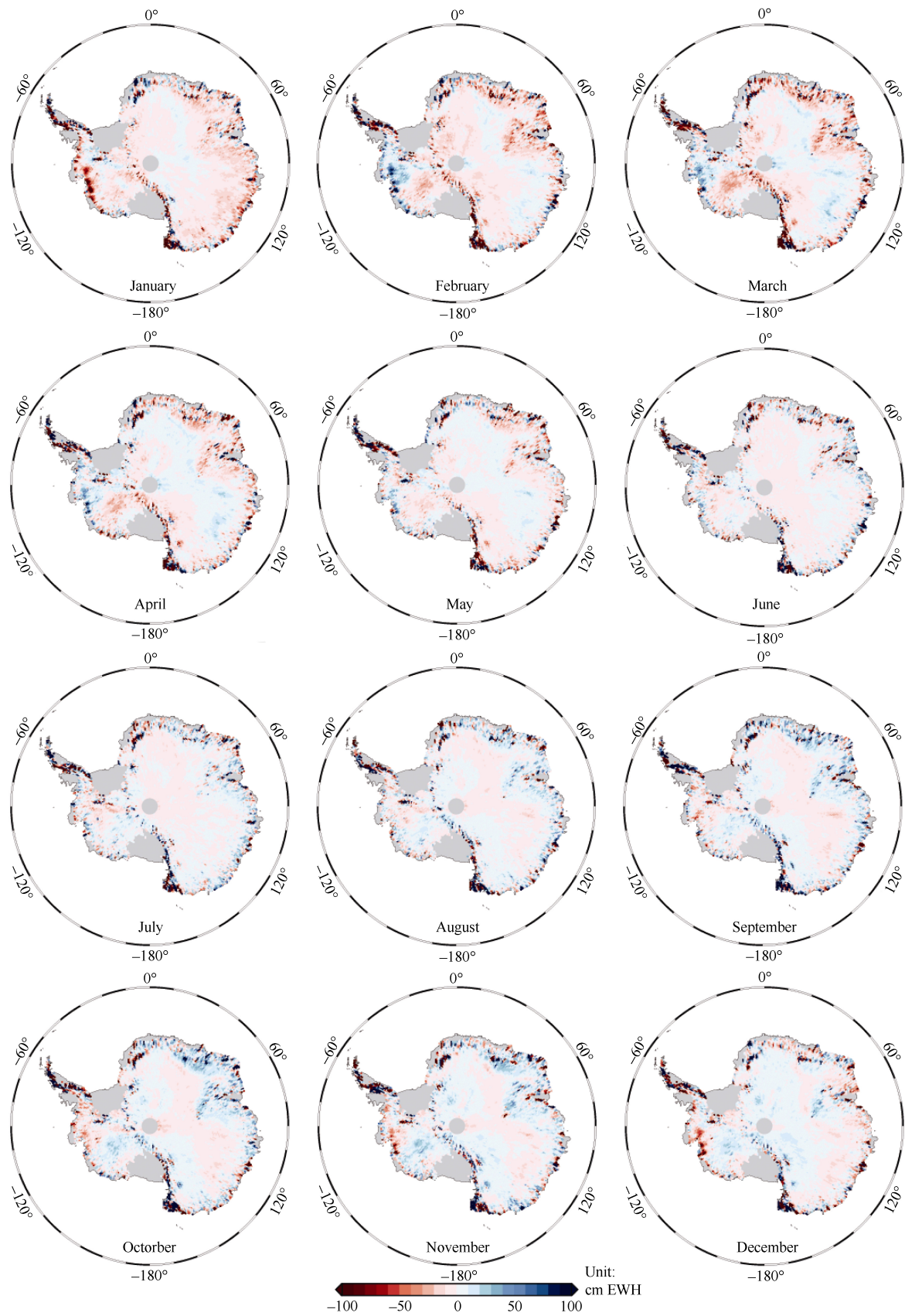
Figure 7 Climatological monthly mass evolution of the AIS between Jan 2011 and Dec 2015, as derived from CryoSat-2.
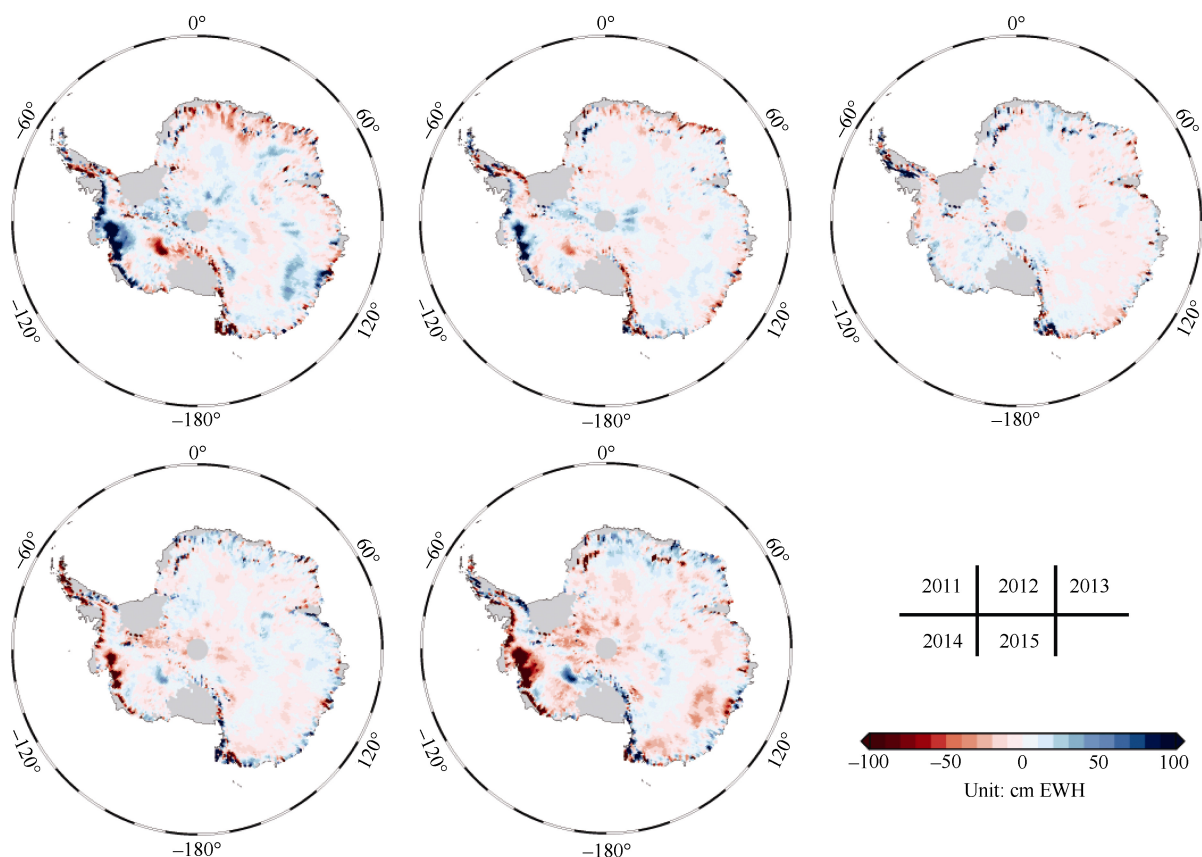
Figure 8   Annual mass evolution of the AIS between Jan 2011 and Dec 2015, as derived from CryoSat-2.

showed increasingly rapid areal mass loss. An area of mass gain with a moderate rate of increase was found between Dronning Maud Land and Enderby Land. In the Kamb Ice Stream, mass gain was limited to a specific area that showed the largest rate of mass gain for the entire AIS. Alternating mass loss and gain has also occurred in northern areas of the Antarctic Peninsula over the five-year period of study.

References

Argus D F, Peltier W R, Drummond R, et al. 2014. The Antarctica component of postglacial rebound model ICE-6G_C (VM5a) based on GPS positioning, exposure age dating of ice thicknesses, and relative sea level histories. Geophys J Int, 198(1): 537–563

Armitage T W K, Wingham D J, Ridout A L. 2014. Meteorological origin of the static crossover pattern present in low-resolution-mode CryoSat-2 data over Central Antarctica. IEEE Geosci Remote Sens Lett, 11(7): 1295–1299

Bamber J L, Gomez-Dans J L, Griggs J A. 2009. A new 1 km digital elevation model of the Antarctic derived from combined satellite radar and laser data-Part 1: Data and methods. Cryosphere, 3(1): 101–111

Boening C, Lebsock M, Landerer F, et al. 2012. Snowfall—driven mass change on the East Antarctic ice sheet. Geophys Res Lett, 39(21): L21501

Chen J L, Wilson C R, Blankenship D, et al. 2009. Accelerated Antarctic ice loss from satellite gravity measurements. Nat Geosci, 2(12): 859–862

Ewert H, Groh A, Dietrich R. 2012b. Volume and mass changes of the Greenland ice sheet inferred from ICESat and GRACE. J Geodyn, 59–60: 111–123

Ewert H, Popov S V, Richter A, et al. 2012a. Precise analysis of ICESat altimetry data and assessment of the hydrostatic equilibrium for subglacial Lake Vostok, East Antarctica. Geophys J Int, 191(2): 557–568

Flament T, Rémy F. 2012. Dynamic thinning of Antarctic glaciers from along-track repeat radar altimetry. J Glaciol, 58(211): 830–840

Gao C C, Lu Y, Zhang Z Z, et al. 2015. Ice sheet mass balance in Antarctica measured by GRACE and its uncertainty. Chinese J Geophys, 58(3): 780–792 (in Chinese)

Gardner A S, Moholdt G, Scambos T, et al. 2017. Increased West Antarctic ice discharge and East Antarctic stability over the last seven years. Cryosphere, doi: 10.5194/tc-2017-75

Groh A, Ewert H, Rosenau R, et al. 2014. Mass, volume and velocity of

the Antarctic ice sheet: present-day changes and error effects. Surv Geophys, 35(6): 1481–1505

Groh A, Ewert H, Scheinert M, et al. 2012. An investigation of Glacial Isostatic Adjustment over the Amundsen Sea sector, West Antarctica. Global Planet Change, 98–99: 45–53

Gunter B, Urban T, Riva R, et al. 2009. A comparison of coincident GRACE and ICESat data over Antarctica. J Geodesy, 83(11): 1051–1060

Gunter B C, Didova O, Riva R E M, et al. 2014. Empirical estimation of present-day Antarctic glacial isostatic adjustment and ice mass change. Cryosphere, 8(2): 743–760

Harig C, Simons F J. 2015. Accelerated West Antarctic ice mass loss continues to outpace East Antarctic gains. Earth Planet Sci Lett, 415: 134–141

Hogg A E, Shepherd A, Cornford S L, et al. 2017. Increased ice flow in Western Palmer Land linked to ocean melting. Geophys Res Lett, 44(9): 4159–4167

Kennicutt II M C, Chown S L, Cassano J J, et al. 2015. A roadmap for Antarctic and Southern Ocean science for the next two decades and beyond. Antarct Sci, 27(1): 3–18

Lenaerts J T M, Van Den Broeke M R, Van De Berg W J, et al. 2012. A new, high-resolution surface mass balance map of Antarctica (1979–2010) based on regional atmospheric climate modeling. Geophys Res Lett, 39(4): L04501

Li F, Yuan L X, Zhang S K, et al. 2016. Mass change of the Antarctic ice sheet derived from ICESat laser altimetry. Chinese J Geophys, 59(1): 93–100 (in Chinese)

Ligtenberg S R M, Helsen M M, Van den Broeke M R. 2011. An improved semi-empirical model for the densification of Antarctic firn. Cryosphere, 5(4): 809–819

Liu J, Xie H, Marco S, et al. 2014. Elevation Changes of East Antarctic Derived from ICESat Laser Altimetry. J Tongji Univ (Nat Sci), 42(11): 1733–1737, 1775 (in Chinese)

Luthcke S B, Sabaka T J, Loomis B D, et al. 2013. Antarctica, Greenland and Gulf of Alaska land-ice evolution from an iterated GRACE global mascon solution. J Glaciol, 59(216): 613–631

McMillan M, Leeson A, Shepherd A, et al. 2016. A high-resolution record of Greenland mass balance. Geophys Res Lett, 43(13): 7002–7010

McMillan M, Shepherd A, Gourmelen N, et al. 2014b. Rapid dynamic activation of a marine—based Arctic ice cap. Geophys Res Lett, 41(24): 8902–8909

McMillan M, Shepherd A, Sundal A, et al. 2014a. Increased ice losses from Antarctica detected by CryoSat-2. Geophys Res Lett, 41(11): 3899–3905

Mouginot J, Rignot E, Scheuchl B. 2014. Sustained increase in ice discharge from the Amundsen Sea Embayment, West Antarctica, from 1973 to 2013. Geophys Res Lett, 41(5): 1576–1584

Pritchard H D, Arthern R J, Vaughan D G, et al. 2009. Extensive dynamic thinning on the margins of the Greenland and Antarctic ice sheets. Nature, 461(7266): 971–975

Pritchard H D, Ligtenberg S R M, Fricker H A, et al. 2012. Antarctic ice-sheet loss driven by basal melting of ice shelves. Nature, 484(7395): 502–505

Rémy F, Parouty S. 2009. Antarctic ice sheet and radar altimetry: a review.

Remote Sens, 1(4): 1212–1239

Rignot E. 2002. Mass balance of East Antarctic glaciers and ice shelves from satellite data. Ann Glaciol, 34: 217–227

Rignot E, Bamber J L, Van Den Broeke M R, et al. 2008. Recent Antarctic ice mass loss from radar interferometry and regional climate modelling. Nat Geosci, 1(2): 106–110

Rignot E, Velicogna I, Van den Broeke M R, et al. 2011. Acceleration of the contribution of the Greenland and Antarctic ice sheets to sea level rise. Geophys Res Lett, 38(5): L05503

Riva R E M, Gunter B C, Urban T J, et al. 2009. Glacial isostatic adjustment over Antarctica from combined ICESat and GRACE satellite data. Earth Planet Sci Lett, 288(3–4): 516–523

Sasgen I, Konrad H, Ivins E R, et al. 2013. Antarctic ice-mass balance 2003 to 2012: regional reanalysis of GRACE satellite gravimetry measurements with improved estimate of glacial-isostatic adjustment based on GPS uplift rates. Cryosphere, 7(5): 1499–1512

Seo K W, Wilson C R, Scambos T, et al. 2015. Surface mass balance contributions to acceleration of Antarctic ice mass loss during 2003–2013. J Geophys Res Solid Earth, 120(5): 3617–3627

Shepherd A, Ivins E R, Geruo A, et al. 2012. A reconciled estimate of ice-sheet mass balance. Science, 338(6111): 1183–1189

Shi H L, Lu Y, Du Z L, et al. 2011. Mass change detection in Antarctic ice sheet using ICESat block analysis techniques from 2003~2008. Chinese J Geophys, 54(4): 958–965 (in Chinese)

Smith W H F, Wessel P. 1990. Gridding with continuous curvature splines in tension. Geophysics, 55(3): 293–305

Sutterley T C, Velicogna I, Rignot E, et al. 2014. Mass loss of the Amundsen Sea Embayment of West Antarctica from four independent techniques. Geophys Res Lett, 41(23): 8421–8428

Velicogna I, Wahr J. 2013. Time-variable gravity observations of ice sheet mass balance: Precision and limitations of the GRACE satellite data. Geophys Res Lett, 40(12): 3055–3063

Wen J H, Wang Y F, Wang W L, et al. 2010. Basal melting and freezing under the Amery Ice Shelf, East Antarctica. J Glaciol, 56(195): 81–90

Wessel P, Smith W H F, Scharroo R, et al. 2017. GMT documentation release 5.4.2. http://gmt.soest.hawaii.edu/doc/5.4.2/index.html

Wingham D J, Francis C R, Baker S, et al. 2006. CryoSat: A mission to determine the fluctuations in Earth's land and marine ice fields. Adv Space Res, 37(4): 841–871

Yan L, Moore J C, Xiao C, et al. 2015. Ocean-driven thinning enhances iceberg calving and retreat of Antarctic ice shelves. Proc Natl Acad Sci USA, 112(11): 3263–3268

Zhang B J, Wang Z M, Li F, et al. 2017. Estimation of present-day glacial isostatic adjustment, ice mass change and elastic vertical crustal deformation over the Antarctic ice sheet. J Glaciol, 63(240): 703–715

Zwally H J, Giovinetto M B, Beckley M A, et al. 2012. Antarctic and Greenland Drainage Systems, GSFC Cryospheric Sciences Laboratory. http://icesat4.gsfc.nasa.gov/cryo_data/ant_grn_drainage_systems.php

Zwally H J, Giovinetto M B, Li J, et al. 2005. Mass changes of the Greenland and Antarctic ice sheets and shelves and contributions to sea-level rise: 1992-2002. J Glaciol, 51(175): 509–527

Zwally H J, Li J, Robbins J W, et al. 2015. Mass gains of the Antarctic ice sheet exceed losses. J Glaciol, 61(230): 1019–1036